International Journal of Pharmaceutics 693 (2026) 126689

Contents lists available at ScienceDirect

International Journal of Pharmaceutics

journal homepage: www.elsevier.com/locate/ijpharm

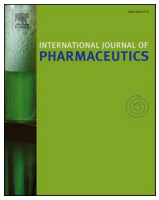

Nanofibers of polyester–polydopamine copolymers enable combined photothermal effect and chemotherapy for local cancer treatment

Giuseppina Biscari [a], Alessia Lo Re [a], Calogero Fiorica [a,*], Vincent Darcos [b], Stéphane Dejean [b], Fabio Salvatore Palumbo [a], Gennara Cavallaro [a], Benjamin Nottelet [b,c,**], Giovanna Pitarresi [a]

[a] Department of Biological Chemical and Pharmaceutical Science and Technology (STEBICEF), University of Palermo, Via Archirafi 30-32, Palermo 90123, Italy
[b] Department of Polymers for Health and Biomaterials, IBMM, Univ Montpellier, CNRS, ENSCM, Montpellier, France
[c] Department of Pharmacy, Nîmes University Hospital, 30900 Nimes, France

ARTICLE INFO

Keywords:
Nanofibers
Electrospun
Polycaprolactone-polydopamine graft copolymer
Doxorubicin
Photothermal therapy
Post-surgical chemotherapy

ABSTRACT

Cancer remains one of the most significant global health challenges, with surgery representing the primary therapeutic approach for most solid tumors. However, the risk of local recurrence due to residual tumor cells necessitates the development of innovative strategies that can provide localized, controlled treatment. This study presents multifunctional electrospun scaffolds based on a poly(ε-caprolactone)-graft-polydopamine (PCL-g-PDA) copolymer blended with polylactic acid (PLA) and loaded with doxorubicin (DOX). Plasma treatment significantly improved the surface wettability of the scaffold. Morphological and physicochemical analyses confirmed the formation of homogeneous fibres. The presence of PDA side chains results in a notable photothermal response when exposed to near-infrared (NIR) light, reaching hyperthermic temperatures of up to 48 °C. Release studies revealed controlled pH-responsive kinetics that were further accelerated by NIR exposure and subsequent thermal activation. *In vitro* assays on HCT-116 colorectal cancer cells cultured in 2D and 3D revealed enhanced cytotoxic effects resulting from the combination of chemotherapy and photothermal therapy. These results demonstrate the significant potential of the PLA/PCL-g-PDA + DOX scaffold as a smart and multifunctional therapeutic platform for localized, potential post-surgical cancer treatment. It effectively combines chemotherapy and hyperthermia to minimize the risk of recurrence.

1. Introduction

Cancer represents one of the major public health challenges today, not only due to its high incidence but also due to the significant socio-economic impact associated with its management. According to data from the GLOBOCAN 2020 project, approximately 19.3 million new cases were diagnosed and approximately 10 million deaths from the disease were recorded (Sung et al., 2021). Despite advances in oncology, surgery remains the treatment of choice for most solid tumors, with the goal of completely removing the primary tumor and potentially involved regional lymph nodes. However, this approach has limitations, such as the possibility of residual tumor cells in the surgical margins, increasing the risk of recurrence and local metastasis (Liu et al., 2022; Zhang et al., 2018). To prevent such events, adjuvant treatments such as chemotherapy and radiotherapy are used, which however involve significant side effects and immunosuppression, with an increased risk of infection and a delay in healing (Ji et al., 2021). In this context, recent technological advances are focused on the development of polymeric systems for post-operative local–regional cancer treatment, such as films, hydrogels, micro/nanoparticles, and patches (Federico et al., 2022; Martorana et al., 2025; Zhang and Jiang, 2021). These systems aim to concentrate the drug they contain in the residual post-operative area, reducing systemic exposure and toxicity to healthy organs. Most of these systems are biodegradable, thus avoiding second surgery and minimizing the risk of chronic immune response (Feng et al., 2023; Langer, 1980; Zhou et al., 2025). This growing interest in polymeric scaffolds

* Corresponding author.
** Corresponding author at: Department of Polymers for Health and Biomaterials, IBMM, Univ Montpellier, CNRS, ENSCM, Montpellier, France.
E-mail addresses: giuseppina.biscari@unipa.it (G. Biscari), alessia.lore@unipa.it (A.L. Re), calogero.fiorica@unipa.it (C. Fiorica), vincent.darcos@umontpellier.fr (V. Darcos), stephane.dejean@umontpellier.fr (S. Dejean), fabiosalvatore.palumbo@unipa.it (F.S. Palumbo), gennara.cavallaro@unipa.it (G. Cavallaro), Benjamin.Nottelet@umontpellier.fr (B. Nottelet), giovanna.pitarresi@unipa.it (G. Pitarresi).

https://doi.org/10.1016/j.ijpharm.2026.126689
Received 16 December 2025; Received in revised form 4 February 2026; Accepted 15 February 2026
Available online 16 February 2026

has spurred the development of various fabrication techniques, including electrospinning. Fibers obtained using this technique are distinguished by their high loading capacity, good encapsulation efficiency, and a porous three-dimensional structure that favors the diffusion of the active agents. They also have a morphology like the extracellular matrix, a large specific surface area, and good biocompatibility, making them particularly suitable for use as implantable devices for localized drug delivery (Zhang et al., 2016) and can be applied directly to the tumor site or along the resection margins, helping to limit recurrence. For example, Kaplan et al. used a network of biodegradable nanofibers made of poly(ε-caprolactone) and poly(glycerol monostearate-co-caprolactone), loaded with cisplatin to prevent lung cancer recurrence after surgical resection, achieving controlled release for up to 90 days and demonstrating effective antitumor activity (Kaplan et al., 2016). A very promising, minimally invasive and highly localized adjuvant strategy for postoperative treatment of cancer is photothermal therapy (PTT). Thanks to its ability to destroy residual tumor cells through heat generated by the conversion of light, it reduces the risk of local recurrence. PTT can be integrated with implantable materials, limiting systemic side effects (Kim et al., 2025). The photothermal materials absorb light in the near-infrared (NIR, 650–1024 nm), generally a wavelength of 808–810 nm is used, and can be inorganic compounds, such as iron oxides and copper or gold-based compounds, or organic compounds, such as carbonaceous materials (graphene, nanotubes), small molecules, such as indocyanine green and polymeric nanomaterials, such as polydopamine (PDA) (Biscari et al., 2025, 2022; Chen et al., 2015; Dar et al., 2025; Fiorica et al., 2021; Hu et al., 2022; MacKey et al., 2014). The inorganic nanoparticles present some critical issues such as non-biodegradability, they can accumulate in the body, and are unsuitable for prolonged or repeated applications, due to fragmentation and fusion (Link et al., 1999). Furthermore, their intrinsic instability complicates their integration into polymer matrices via electrospinning (Han et al., 2012). Consequently, biocompatible organic materials are attracting much attention, especially because they can perform multiple functions, such as controlled drug release triggered by pH and/or NIR light, hyperthermic effect, high physiological stability, and compatibility with drug-loaded fibrous matrices. Among these materials, PDA certainly stands out for its excellent photothermal properties, biocompatibility, and chemical versatility, making it particularly suitable for post-surgical oncological applications (Du et al., 2022; Fernandes et al., 2025; Hou et al., 2025; Wang et al., 2022). For example, Tiwari et al. produced polycaprolactone (PCL)-based fibrous membranes loaded with Doxorubicin (DOX) and coated with multistimuli-responsive (pH/NIR) PDA, to achieve a combined therapeutic system (chemotherapy + hyperthermia) on a single platform (Tiwari et al., 2019). Despite their potential, PDA-based nanomaterials have limitations, including the risk of undesired release and aggregation, and the requirement for additional synthetic steps to incorporate them into polymer matrices. Furthermore, since PDA is not soluble, it is used only as a coating or nanoparticles incorporated into polymer matrices, thus resulting in composite materials (Abounahia et al., 2022; Ding et al., 2014; Lee et al., 2020; Mahmoud et al., 2021; Sy et al., 2018; Yan et al., 2015). Although PDA has already been used in fibrous membranes for localized drug delivery in photothermal therapy, to our knowledge, its use in nanofibrous membranes produced using a polymer directly functionalized with PDA chains has not yet been reported. Bahuon et al. synthesised a PDA-grafted PCL (PCL-g-PDA) thermoplastic copolymer, which presents PDA side chains directly attached to the polyester backbone. This material, that can be processed like any thermoplastic, has demonstrated the ability to load and release drugs such as dexamethasone and ciprofloxacin hydrochloride in a controlled and extended manner thanks to interactions between drugs and PDA (Bahuon et al., 2022).

This work therefore aims to develop a smart multifunctional electrospun scaffold based on this PCL-g-PDA thermoplastic copolymer in combination with poly(lactic acid) (PLA), capable of releasing DOX, activated by pH and NIR irradiation. The key innovation is the demonstration that integrating PDA pendant chains covalently anchored to the PCL backbone endows the matrix with a stable photothermal response. Under NIR irradiation, PDA converts light into heat, softening the fibers and accelerating DOX release, allowing on/off control of drug release. This intrinsic photothermal capacity enables heat generation for the potential combined post-operative hyperthermic cancer treatment. This system has demonstrated high efficacy in damaging tumor cells, as demonstrated by in vitro studies performed on 2D and 3D cultures of HCT-116 cells, making it a promising solution for combined photothermal and chemotherapy therapies.

2. Materials and methods

2.1. Chemicals

Dimethyl sulfoxide (DMSO), dichloromethane (DCM), N,N-dimethylformamide (DMF), doxorubicin (DOX), Dulbecco's Minimum Essential Medium (DMEM), CellTiter 96® AQueous One Solution Cell Proliferation Assay (MTS), and Live/Dead Cell Double Staining Kit were purchased from Sigma-Aldrich (Italy). D,L-polylactic acid (PLA) 230 kDa was purchased from Bidachem-Boeringher Ingelheim. PCL-g-PDA was synthesized as previously reported (Bahuon et al., 2022) with exception of the purification procedure that was modified to improve the yield (53%). The detailed synthesis procedure is provided as supplementary information.

2.2. Production of the PLA/PCL-g-PDA + DOX scaffold

Three different solutions had to be prepared extemporaneously to obtain a mixture for electrospinning. The first was obtained by dispersing PLA at 7% w/v in DCM, the second by dispersing PCL-g-PDA at 7% w/v in DMF, and the last by solubilizing DOX at 1.5% w/v in a DMSO: DMF mixture (1:6). The prepared dispersions were then mixed until complete homogenization. The electrospinning process was conducted using a KDScientific Mod. 78-8100INT programmed-flow pump and a Spellman CZE1000R high-voltage generator (Pitarresi et al., 2022). The rotating metal collector was a custom design. The solution was loaded into a 1 ml plastic syringe equipped with a 0.52 mm internal diameter metal needle (21G). The optimal flight space, measured from the needle tip to the collector, was approximately 15 cm. The solution flow rate was set to 0.02 ml/min using a programmable automatic pump with a housing to secure the syringe during the process. A voltage of 20 kV was applied using a dedicated high-voltage generator. The resulting fibrillar scaffolds, named PLA/PCL-g-PDA, were collected on non-woven fabric (TNT) sheets and fixed to a rotating metal collector (3.8 cm in diameter at 300 rpm). Three different control electrospun scaffolds were produced maintaining the same polymer concentrations, ratios and the same instrumental conditions, one without DOX called PLA/PCL-g-PDA, another using PLA and a 45 kDa PCL without DOX, called PLA/PCL and a last one in which DOX was present instead, called PLA/PCL + DOX. The scaffolds obtained were stored at −20 °C until analysis.

2.3. Plasma treatment of the scaffold

The scaffolds were treated with a low-pressure cold plasma device using nitrogen gas, manufactured by Diener (Model FEMTO-B), coupled to a Pfeiffer PBF 71/2B-11RQ vacuum pump. The scaffolds were introduced into the device's vacuum chamber. After creating a vacuum (0.4 mbar), the chamber was saturated with nitrogen gas (Pin = 1 bar, flow rate = 15 ml/min) until the pressure inside the chamber was between 1 and 1.5 mbar. Once these parameters were reached, the generator was activated for 15 min at 80% power.

2.4. Physical characterization of electrospun scaffolds and release studies

SEM images of electrospun scaffolds were obtained using a Phenom

XL instrument, Alfatest.

Fluorescence microscopy analyses to confirm the presence of DOX within the electrospun scaffolds were performed using a Carl Zeiss AxioVert200 optical microscope.

To study the wettability of the scaffolds, contact angle measurements were performed using the Contact Angle 1000C FTA instrument.

Differential scanning calorimetry (DSC) was conducted with the DSC 131 EVO instrument, SETARAM, heating the samples from 20 °C to 480 °C with a ramp rate of 10 °C/min.

To study the uniaxial mechanical properties of the scaffolds, tests were performed by cutting them into strips (2 × 7 mm) and testing them using the Bose TA Instruments ElectroForce Test Bench System equipped with a 225 N load cell at 10 mm/min at room temperature.

To study photothermal conversion capacity, the scaffold was prepared as described, cut (0.8 cm x 0.8 cm) to obtain approximately 10 mg samples, and placed in 24-well plates. 2 ml of DPBS (pH 7.4) was added to each well. Each sample was irradiated with NIR light at a wavelength of 810 nm (Medical Diode Laser System GBox-15A/B) using three different irradiation powers (1.96, 2.75, and 3.54 W/cm2), monitoring the temperature increase using a CEM Discover SP fiber-optic temperature probe (±0.2 °C) at various times (3, 6, and 9 min).

To study the DOX Encapsulation Efficiency each electrospun sample (5 mg) was immersed in 2 mL of ethanol and incubated at 37 °C with horizontal shaking at 80 rpm for 24 h. After incubation, the DOX concentration was determined using a UV–vis spectrophotometer (Shimadzu UV-2401PC). A standard calibration curve (from 1.15 to 148 μm/ml) for DOX in ethanol was previously prepared to convert absorbance values into concentration. The encapsulation efficiency was calculated using the following Equation:

$$EE\% = A / B \cdot 100$$

A: Amount of drug extracted, B: Total amount of drug initially added during formulation.

Release studies were conducted on the scaffolds, named PLA/PCL + DOX and PLA/PCL-g-PDA + DOX, prepared as described were immersed in 2 ml of DPBS at pH 7.4 and pH 5 at 37 °C. At predetermined times (1, 2, 5, 6, 7, 8, 11, and 15 days), the medium in each well was removed and changed with fresh medium, and the samples were then placed under the same conditions. In another experiment, each sample was subjected to daily NIR treatment at a power of 3.54 W/cm^2 for 9 min for up to 3 days, and the release was compared with that of unirradiated samples. The amount of DOX released over time was determined by UV–vis readings at 480 nm (Shimadzu UV-2401PC) of the collected media.

2.5. In vitro cytotoxicity

For cytotoxicity studies, HCT116 cells (human colorectal carcinoma cell line) were grown in DMEM supplemented with 1% v/v glutamine solution, 1% v/v penicillin streptomycin solution, 10% v/v fetal bovine serum (FBS), and 0.1% v/v amphotericin B solution. The cells were grown at 37 °C in a controlled atmosphere containing 5% CO_2. After treatment with trypsin, the cells were resuspended in DMEM and counted using a Burker chamber method. The experiment was performed by seeding 2 x 10^4 cells in each well of a multiwell plate. After 24 h of incubation, PLA/PCL-g-PDA, PLA/PCL-g-PDA + DOX and PLA/PCL + DOX samples (5 mg each), previously sterilized by UV light (254 nm), were added to the wells with the cells. For each sample type, three replicates were subjected to NIR irradiation (9 min at 3.54 W/cm2), while three others were kept as non-irradiated controls. After a further 24 h of incubation, the MTS assay was performed, following the manufacturer's instructions. At the end of the test, the samples were recovered and reused in a similar manner for a second experimental cycle: the previous day, new cells (2 × 104 per well) had been seeded in another plate, and on the day of the MTS test, the previously used samples were transferred to these fresh cells and incubated for 24 h. Again, three samples were irradiated with NIR light (9 min at 3.54 W/cm2) and three were kept as controls. After 24 h, the MTS assay was performed. The procedure was repeated for a total of three consecutive cycles, using the same samples each time. This allowed cell viability to be assessed after 24, 48, and 72 h of incubation, both in the absence and presence of NIR treatment.

2.6. In vitro anticancer activity on 3D models

The antitumor efficacy of PLA/PCL-g-PDA + DOX scaffolds was further evaluated on 3D spheroids composed of HCT-116 cells, generated using the hanging drop method. Briefly, 20 μL of a cell suspension (density of 100 cells μL^{-1}) enriched with 2.5% w/v ECM gel (Corning® Matrigel® Matrix) was deposited on the upper side of a 48-well plate. The resulting spheroids were cultured for four days, with the daily addition of 5 μL of fresh culture medium. On the fourth day, the spheroids were transferred to the wells, placing them in direct contact with the PLA/PCL-g-PDA + DOX scaffolds (5 mg), immersed in fresh culture medium. Untreated spheroids served as negative controls. The potential photothermal activity of the scaffolds was then evaluated. They were kept in direct contact with the spheroids and irradiated with NIR light (810 nm) for 9 min at a power of 3.54 W cm^2 daily. Photothermal ablation was quantified by acquiring microscopic images at different time points (24 h, 3 and 4 days), evaluating the reduction in spheroid volume, calculated according to the following relationship:

$$V = L \cdot W^2 / 2$$

where L represents the largest diameter and W the diameter perpendicular to it. Finally, DOX penetration and internalization within the spheroids were assessed by fluorescence microscopy (Axio Cam MRm, Zeiss), using the Texas Red filter.

2.7. Statistical analysis

All experimental procedures were performed in triplicate, and the results are expressed as mean ± standard deviation. When applicable, the statistical analysis for significance was conducted with the student's *t*-test; values with $p < 0.05$ were considered statistically significant (*$p < 0.05$; **$p < 0.01$; ***$p < 0.001$).

3. Results and discussion

3.1. Production and physical characterization of electrospun scaffolds

The PCL-g-PDA copolymer, synthesized as previously reported (Bahuon et al., 2022), was selected for its pendant PDA side chains, which can establish noncovalent interactions (π-π, hydrogen, electrostatic) with pharmacologically active molecules, such as DOX, promoting its immobilization in the matrix and controlled release (Li et al., 2017b). The intrinsic photothermal properties of PDA, expected to be present in the PDA side chains of PCL-g-PDA, could further confer potential for combined therapeutic applications based on drug release and localized hyperthermia. Due to the low molecular weight of PCL-g-PDA (46 kDa), the copolymer was blended with high molecular weight PLA (230 kDa) in a 1:1 ratio to improve the processability during the electrospinning process. At the same time, DOX was incorporated into the polymer mixture to obtain PLA/PCL-g-PDA + DOX multifunctional scaffolds (Fig. 1) with structural, release, and photothermal properties. The same procedure was used to produce PLA/PCL-g-PDA, PLA/PCL and PLA/PCL + DOX as control scaffolds.

PLA and PCL-based scaffolds are widely used in the biomedical field for their mechanical properties, biodegradability, and biocompatibility. Their lipophilic nature reduces their wettability and can limit biological interaction and the release of active agents (Esmaeili Ranjbar et al., 2025). To overcome this limitation, the samples were treated with low-

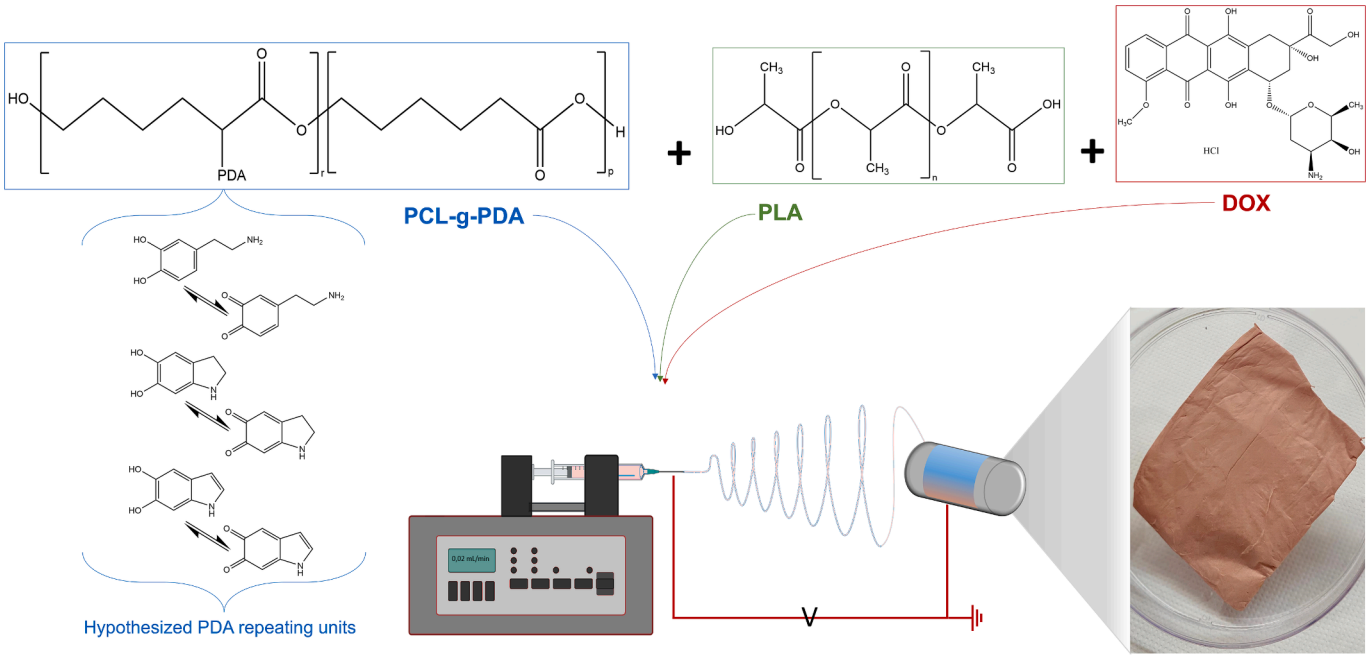

Fig. 1. Scheme of production of PLA/PCL-g-PDA + DOX scaffolds by electrospinning.

pressure cold plasma in a nitrogen-saturated chamber. Plasma activation generated reactive species that introduced surface amino groups, increasing wettability, as evidenced by the reduction of the contact angle of the PLA/PCL-g-PDA scaffold from 108.16° to 68.24°, indicating a clear transition to hydrophilicity (Fig. 2). The complete absorption of the droplet within five seconds further confirmed the effectiveness of the treatment. These results demonstrate that the treatment introduced surface functional groups, increasing wettability and making the material more suitable for biomedical applications. The increased wettability of the electrospun scaffold could in fact improve contact with the tissues, thanks to a more effective interaction with biological fluids, favoring a uniform and prolonged distribution of the chemotherapy on the residual surgical site, with greater local efficacy and fewer systemic effects (Abbasi et al., 2014; Bu et al., 2019; Khodadadi et al., 2020).

The morphological characteristics of the scaffolds were evaluated by SEM (Fig. 3). The images show that in all samples the fibers are distributed homogeneously and randomly, forming a defect-free three-dimensional network. Dimensional analysis indicates that the average fiber diameter depends mainly on the polymer composition, with no significant variations attributable to the plasma treatment. In particular,

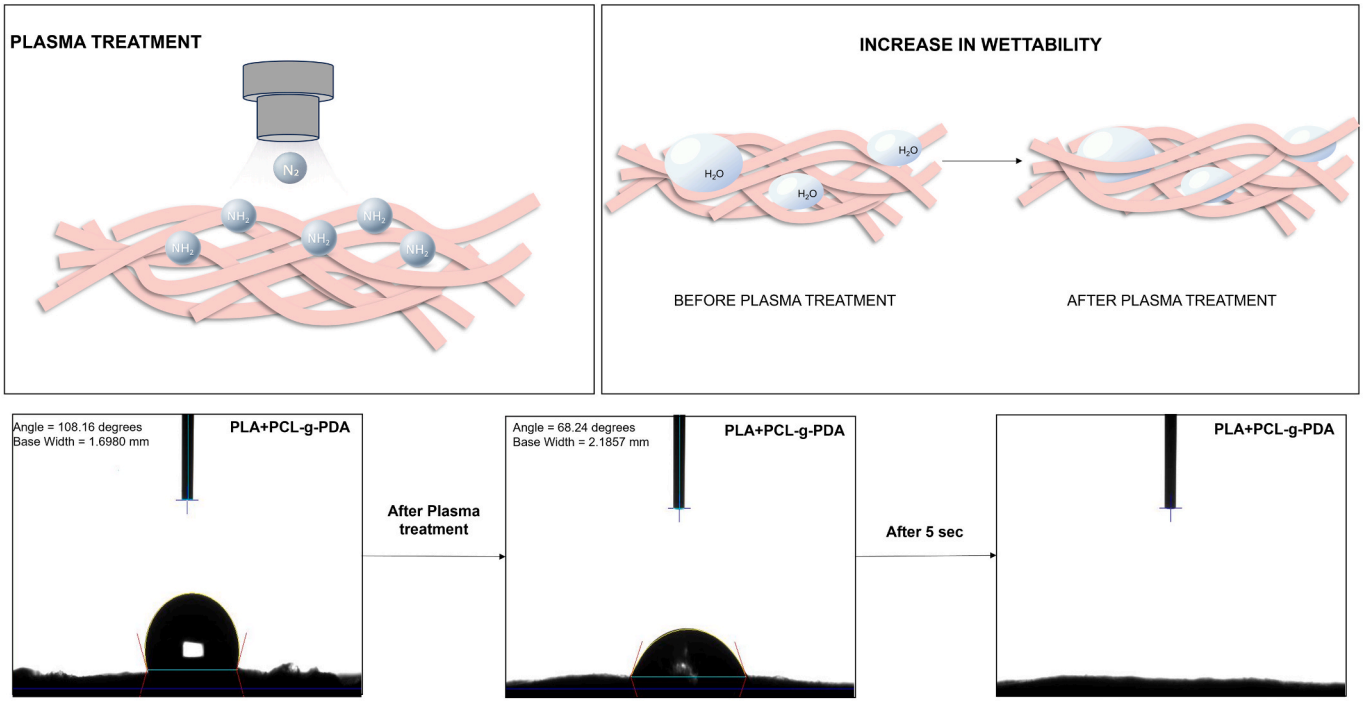

Fig. 2. Schematic representation of plasma treatment and contact angle evaluation of PLA/PCL-g-PDA scaffold before and after plasma treatment.

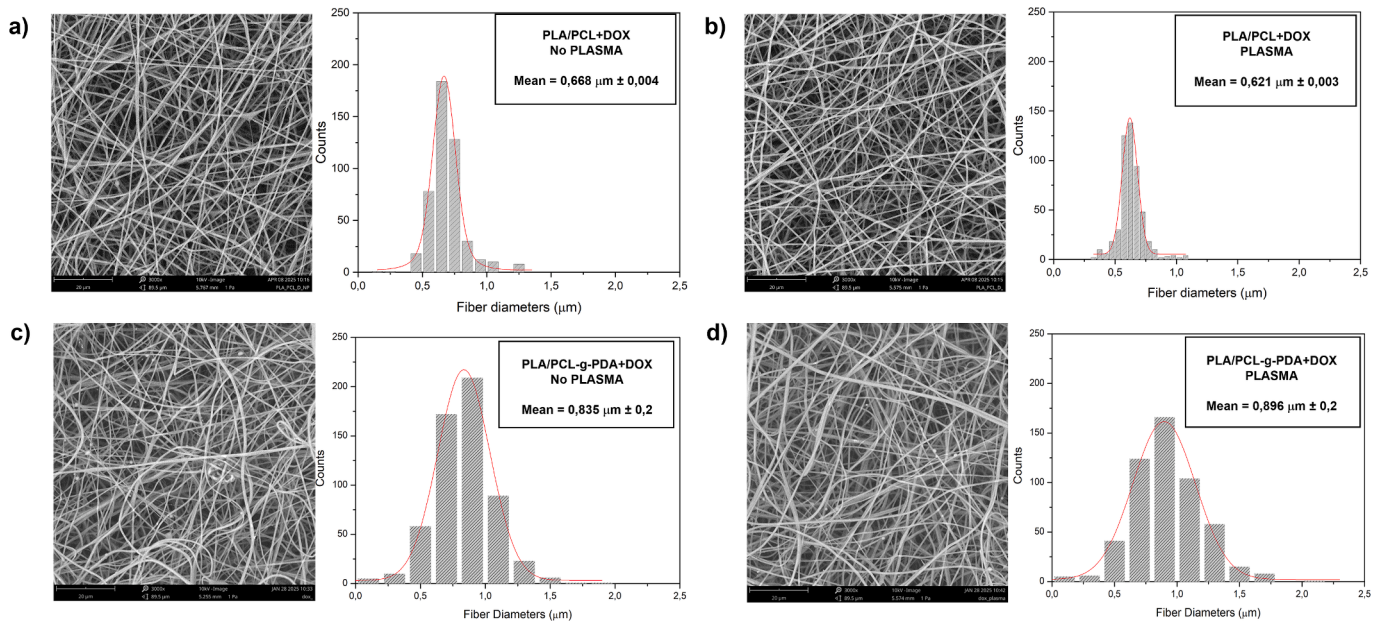

Fig. 3. SEM images of PLA/PCL + DOX scaffolds as unplasma-treated sample (**a**) and as plasma-treated sample (**b**); PLA/PCL-g-PDA + DOX as unplasma-treated sample (**c**) and as plasma-treated sample (**d**). Next to each SEM image, the corresponding histogram is shown, showing the fiber diameter distribution in the different scaffolds.

the average fiber diameters are reported in Table 1.

3.2. Mechanical, thermal characterization and drug encapsulation efficiency of the electrospun scaffold

The presence of DOX was confirmed by fluorescence microscopy on drug loaded PLA/PCL-g-PDA scaffolds (**Fig. S1**). The PLA/PCL-g-PDA + DOX sample was compared with the PLA/PCL-g-PDA sample. While the former showed clear emission on the Texas Red channel, demonstrating the actual presence and homogeneous distribution of DOX within the scaffold, the latter showed no signal, also confirming the absence of autofluorescence of the polymers.

Encapsulation efficiency (EE%) values, calculated following ethanol extraction, were found to be close to 100% (150 μg DOX/10 mg polymers content), indicating highly effective drug incorporation during the manufacturing process. Regarding the concentration of DOX loaded in the electrospun composite, the system obtained here has a concentration of approximately 1.5 wt% with respect to the polymers of which the system is composed. Compared to literature, the PLA/PCL-g-PDA + DOX electrospun mat is classified as a system containing an intermediate amount of DOX compared to the concentrations normally used. For example, in the previously cited work, the fibers produced from PCL and with PDA coating were loaded with Doxorubicin at 10 wt% with respect to the polymer and the EE% was 90 and 75% for the two types of DOX-loaded fibers produced (Tiwari et al., 2019). While in another work, in which it is loaded together with another drug, regenerated silk fibroin (RSF) nanofibers are loaded at 0.1 wt% (Li et al., 2017a).

For the thermal properties, the scaffolds were analyzed by Differential Scanning Calorimetry (DSC), **Fig. S2** shows the thermograms, in which an endothermic peak between 50 and 60 °C is observed in all samples. This is attributable to the melting of the PCL crystalline phase. A peak around 150 °C is also observed, which could correspond to either the melting point of PLA or of PDA (Aldhafeeri et al., 2022; García-Mayorga et al., 2023; Xu et al., 2017). The absence of the typical sharp endothermic peak corresponding to the melting point (Tm) of DOX, which is usually found at around 220 °C and provides evidence of the crystalline structure of the drug, confirmed the presence of DOX in a molecular state within the polymeric matrix (Doustgani, 2017; Shafique et al., 2023).

Although PLA and PCL are both linear aliphatic polyesters, differences in their molecular structure give PCL greater flexibility, hydrophobicity, and crystallinity, resulting in a slower degradation rate than PLA, while the latter exhibits greater stiffness and mechanical strength. It is well known in the literature that combining the two polymers in blends allowing for the modulation of properties such as material degradation times and mechanical behavior . In particular, the use of PLA and PCL blends in the production of scaffolds has been associated with a reduction in degradation times and improved mechanical properties compared to pure PCL scaffolds, making these blends a widely studied and established platform for biomedical applications (Sun and Downes, 2009; Yao et al., 2017). To evaluate the mechanical properties of the scaffolds, tensile tests were performed to analyze peak stress and breaking strain. The PLA/PCL scaffold exhibited a peak stress of 0.35 ± 0.08 MPa, representing the maximum stress the material can withstand before breaking and thus indicating its mechanical strength. In contrast, the PLA/PCL-g-PDA scaffold exhibited a peak stress of 0.29 ± 0.02 MPa (Fig. 4a). Regarding breaking strain, which reflects maximum deformation before fracture and provides a measure of flexibility and mechanical adaptability, values of 59.01% ± 9.8% and 34.01% ± 8.7% were recorded for the PLA/PCL and PLA/PCL-g-PDA scaffolds, respectively (Fig. 4b). Although there are no significant differences in peak stress values, the differences on the breaking strain values observed between the two scaffolds are likely attributable to the grafting of PDA onto the PCL chain. Since PCL is the most ductile component of the system and contributes most to the deformation capacity compared to PLA, which is more brittle, the presence of PDA may interfere with the continuity of the PCL phase, resulting in an overall reduction in breaking strain value (Fernández et al., 2017; Innocent Matumba et al., 2024; Min et al., 2024).

Table 1
The scaffold average fiber diameters.

	No plasma treatment	After plasma treatment
PLA/PCL + DOX	0.668 μm ± 0.004	0.621 μm ± 0.003
PLA/PCL-g-PDA + DOX	0.835 μm ± 0.2	0.896 μm ± 0.2

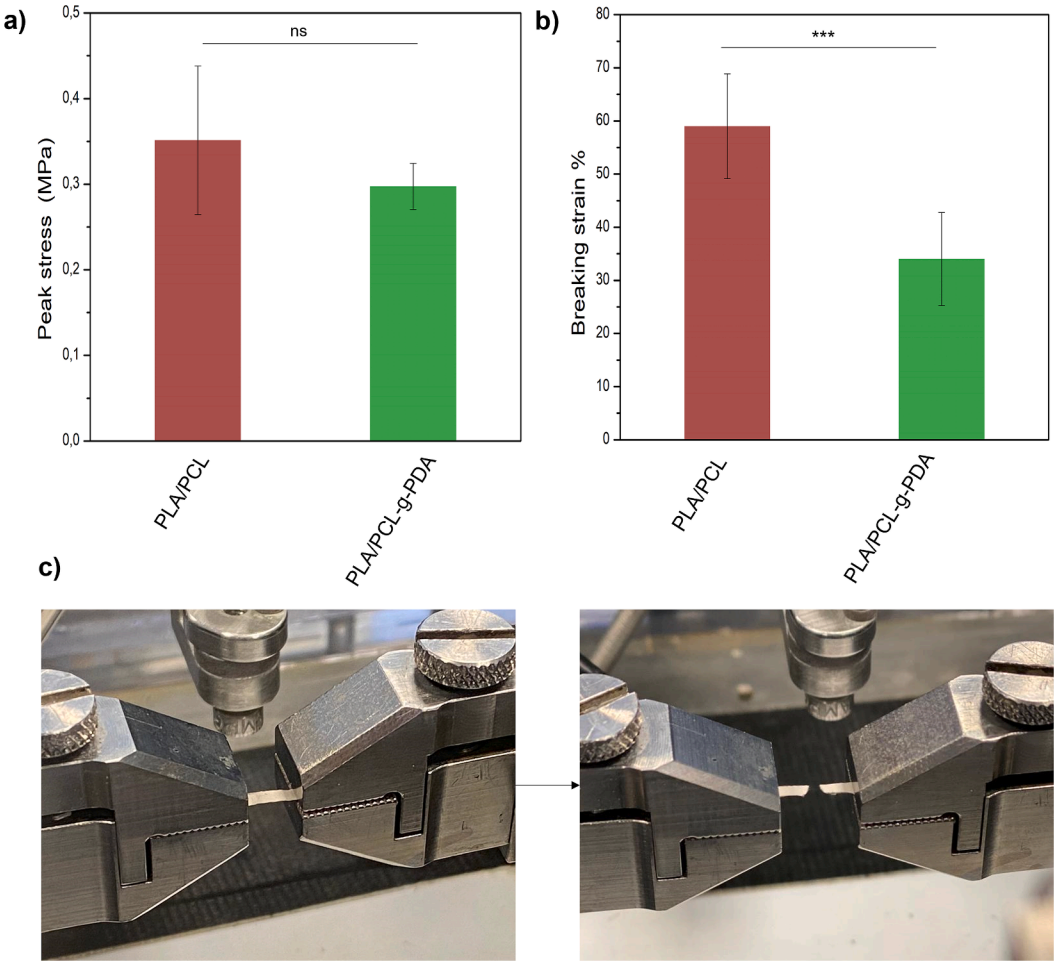

Fig. 4. Peak stress (**a**) and breaking strain % (**b**) of PLA/PCL and PLA/PCL-g-PDA scaffolds. Photos showing the mechanical test (**c**). All data are shown as mean value ± SD (n = 3), (ns $p > 0.05$, ***$p < 0.001$).

3.3. Photothermal properties and drug release studies

The presence of PDA on the PCL-g-PDA backbone endowed the polymer with photothermal properties. As shown in Fig. 5, the temperature of the medium in which the scaffold was placed increased under irradiation with NIR light (808 nm) at three different powers. The results showed a direct correlation between irradiation power, exposure duration and local thermal increase, enabling the photothermal response to be modulated as required. With a power of 1.96 and 2.75 W/cm^2, the temperature increased to 43 °C and 45 °C in 9 min, respectively. With a power of 3.54 W/cm^2, the temperature increased to 44 °C within 6 min and to 48 °C within 9 min, demonstrating effective photothermal conversion. The temperature increased with time and applied power, reaching the therapeutic window for hyperthermia (shown in purple in Fig. 5a). These data confirm the high photothermal conversion capacity of the PCL-g-PDA and the ability to precisely modulate the final temperature by varying the irradiation power and duration. Furthermore, Fig. 5b shows that no significant attenuation of the temperature change occurred under NIR light irradiation for three irradiation-cooling cycles, demonstrating that the photothermal performance of the scaffold remains stable after repeated irradiation.

The PDA-containing electrospun fibers are generally obtained through two-step approaches. In these approaches, PDA is introduced after fiber formation through surface coating processes, or pre-synthesized PDA nanoparticles are incorporated into the electrospinning solution (Atabey et al., 2026; Chen et al., 2022; Deng et al., 2019; Yang and Lee, 2024). However, the PDA is only physically adsorbed or dispersed, which limits the uniformity of distribution and the reproducibility of functional properties. This is because the PDA layer can delaminate or the nanoparticles can aggregate and potentially be released over time, like other photothermal agents (Liu et al., 2025). In the PCL-g-PDA the PDA side chains are covalently linked to the polymer backbone and are integral part of the macromolecular structure of the resulting thermoplastic. This can ensure homogeneous distribution of functional groups and preserves PDA properties such as absorption of NIR light and consequent photothermal conversion of light energy into heat. The experimental demonstration of the photothermal effect in an electrospun material based on a polyester copolymer grafted with PDA pendant caps is, to our knowledge, the first evidence of this behavior in literature. This is a significant result because it shows that photothermal activity does not require nanoparticles or an external PDA coating; it can be intrinsic to the material if it is designed appropriately at a molecular level. This approach eliminates the potential risk of nanoparticle release and ensures reproducible photothermal behavior. It also maintains functionality even after repeated exposure cycles thanks to the covalent bond between the PDA and the PCL backbone.

Fig. 5c shows the release of DOX from the PLA/PCL + DOX and PLA/PCL-g-PDA + DOX scaffolds. The release, evaluated at pH 5.0 and 7.4, is lower in the PDA scaffold and strongly influenced by the acidity of the medium. Drug release, especially from the PLA/PCL + DOX scaffolds at both pH 5 and pH 7.4 and the PLA/PCL-g-PDA + DOX scaffold at pH 5, showed a biphasic profile, with an initial burst release lasting up to 48 h; the subsequent time interval showed a slow and sustained release at all pH conditions. While the PLA/PCL-g-PDA + DOX scaffold at pH 7.4 did

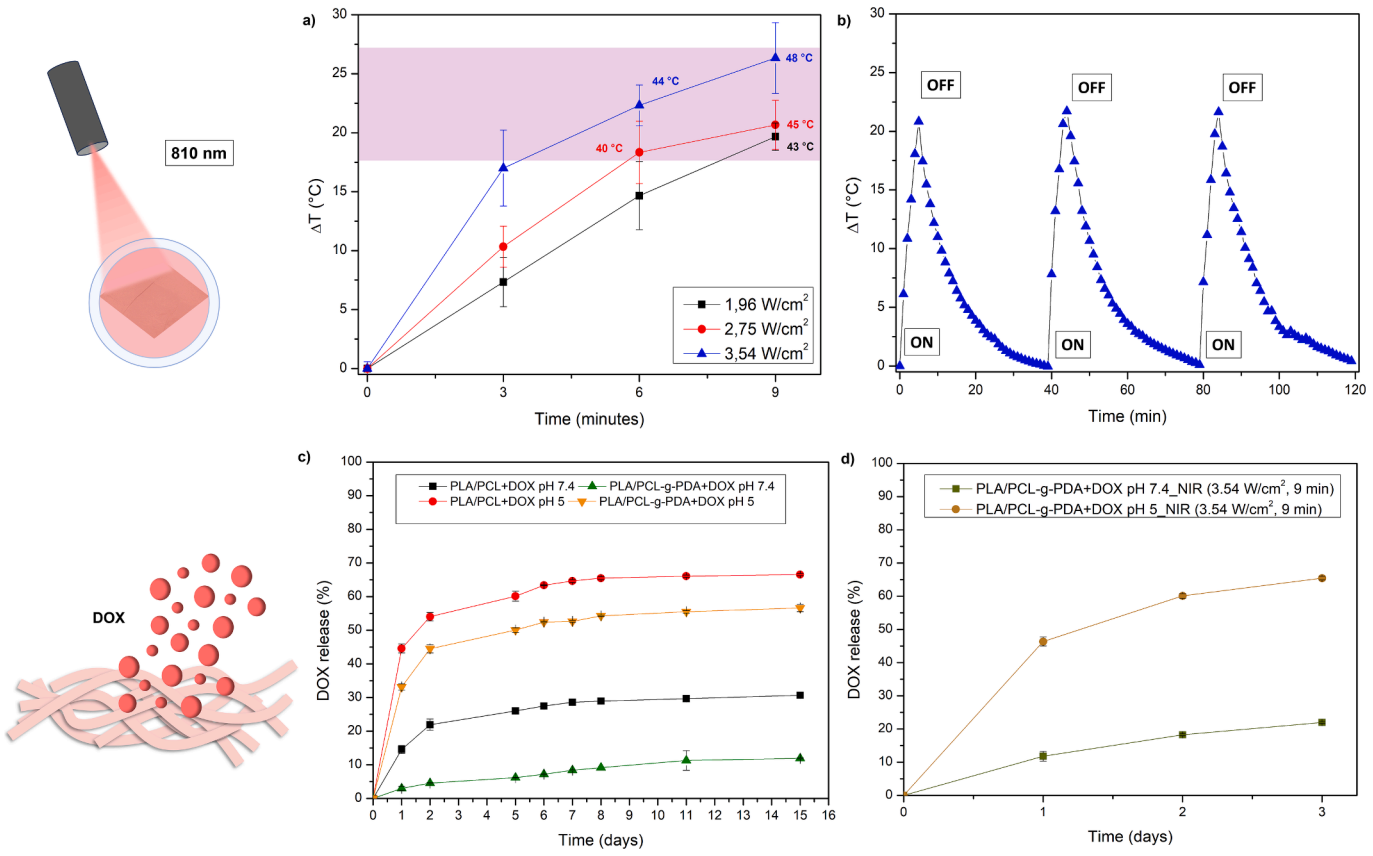

Fig. 5. Photothermal conversion capability of the PLA/PCL-g-PDA scaffold under NIR-light irradiation at different powers (1.96, 2.75, 3.54 W/cm^2) (**a**), and during irradiation-cooling cycles with NIR light (5 min for irradiation and 35 min for cooling) at a power of 3.54 W/cm^2 (**b**). Release of DOX from PLA/PCL-g-PDA + DOX and PLA/PCL + DOX in DPBS at pH 7.4 and 5 (**c**) and after daily NIR irradiation treatment (3.54 W/cm^2, 9 min) (**d**). All data are shown as mean value ± DS (n = 3).

not show this initial burst release, but only a very slow, sustained release that was lower than the other conditions. After 14 days, at pH 7.4, ~10% of DOX is released from the PLA/PCL-g-PDA + DOX scaffold and ~ 30% from the PLA/PCL + DOX scaffold, while at pH 5.0 the percentages increase to ~ 55% and ~ 65%, respectively. The greater solubility of DOX at acidic pH resulted in easier diffusion of the drug from the scaffold. Therefore, this pH-sensitive behavior could be exploited because it allows for limited release under physiological conditions, reducing side effects, and more intense release in the acidic environments typical of tumor recurrence (Abasalta et al., 2022; Rezk et al., 2024; Tiwari et al., 2019). The presence of PDA confers the advantage of retaining the drug to a greater extent than the control PLA/PCL + DOX scaffold, confirming that PDA establishes π–π interactions with DOX, contributing to a more controlled and potentially safer release, making this approach particularly promising for locoregional delivery applications in oncology (Bahuon et al., 2022; Tiwari et al., 2019; Tran et al., 2015). The effect of NIR light on the PLA/PCL-g-PDA scaffold in DPBS was studied under the same different pH conditions used previously. PLA/PCL-DOX did not exhibit heating properties; therefore, these fibers were excluded from NIR irradiation treatment for release studies. NIR irradiation (810 nm, 3.54 W/cm^2, 9 min, daily) induces a thermal increase that accelerates drug diffusion. In fact, as shown in Fig. 5d, after only 72 h, DOX release from the PLA/PCL-g-PDA + DOX scaffold reaches ~ 20% at pH 7.4 and ~ 65% at pH 5. These results demonstrate that NIR irradiation could enhance the therapeutic efficacy of the scaffold in a dual way, on the one hand, by promoting an increase in DOX release, on the other, by inducing a local hyperthermic effect, known for its enhanced action in damaging tumor cells. In this sense, the PLA/PCL-g-PDA + DOX scaffold, thanks to the presence of PDA, not only acts as a controlled release system, but also appears as a multifunctional platform with potential application in combined chemo-photothermal therapy.

3.4. *Biological evaluation*

To evaluate the cytotoxic effect of the PLA/PCL-g-PDA + DOX scaffold, colorectal cancer cells (HCT-116) were used. Considering that this system could exert a combined antitumor action through the controlled release of DOX and the hyperthermic action induced by NIR irradiation, cell viability was monitored in the presence of the samples, also by subjecting them to NIR treatment. At each time point studied, the previously used samples were transferred to plates containing fresh cell cultures, with which they remained in contact until the next point of the assay, as shown in the scheme in Fig. 6a. The drug-free PLA/PCL-g-PDA and PLA/PCL + DOX scaffolds were used as controls. Fig. 6b shows that the PLA/PCL-g-PDA scaffold significantly reduces cell viability following NIR irradiation (~ 65% on average across the three time points studied) compared to the unirradiated condition (~ 92% on average across the three time points studied). This result confirms that the hyperthermic effect induced by PDA is sufficient to cause cell damage and death due to thermal stress. In the absence of irradiation, cells exposed to the PLA/PCL-g-PDA + DOX and PLA/PCL + DOX scaffolds show comparable viability values across all time points analyzed (~ 40% on average across the three time points studied). Conversely, NIR irradiation induces a greater reduction in viability in the PLA/PCL-g-PDA + DOX (~ 25% on average across the three time points studied), thanks to the hyperthermic effect caused by the presence of PDA. This result demonstrates that hyperthermia enhances the action of chemotherapy, amplifying the overall antitumor effect. Morphological observations obtained by light microscopy (Fig. 6c) corroborate the quantitative data; in fact, cells treated with DOX-loaded

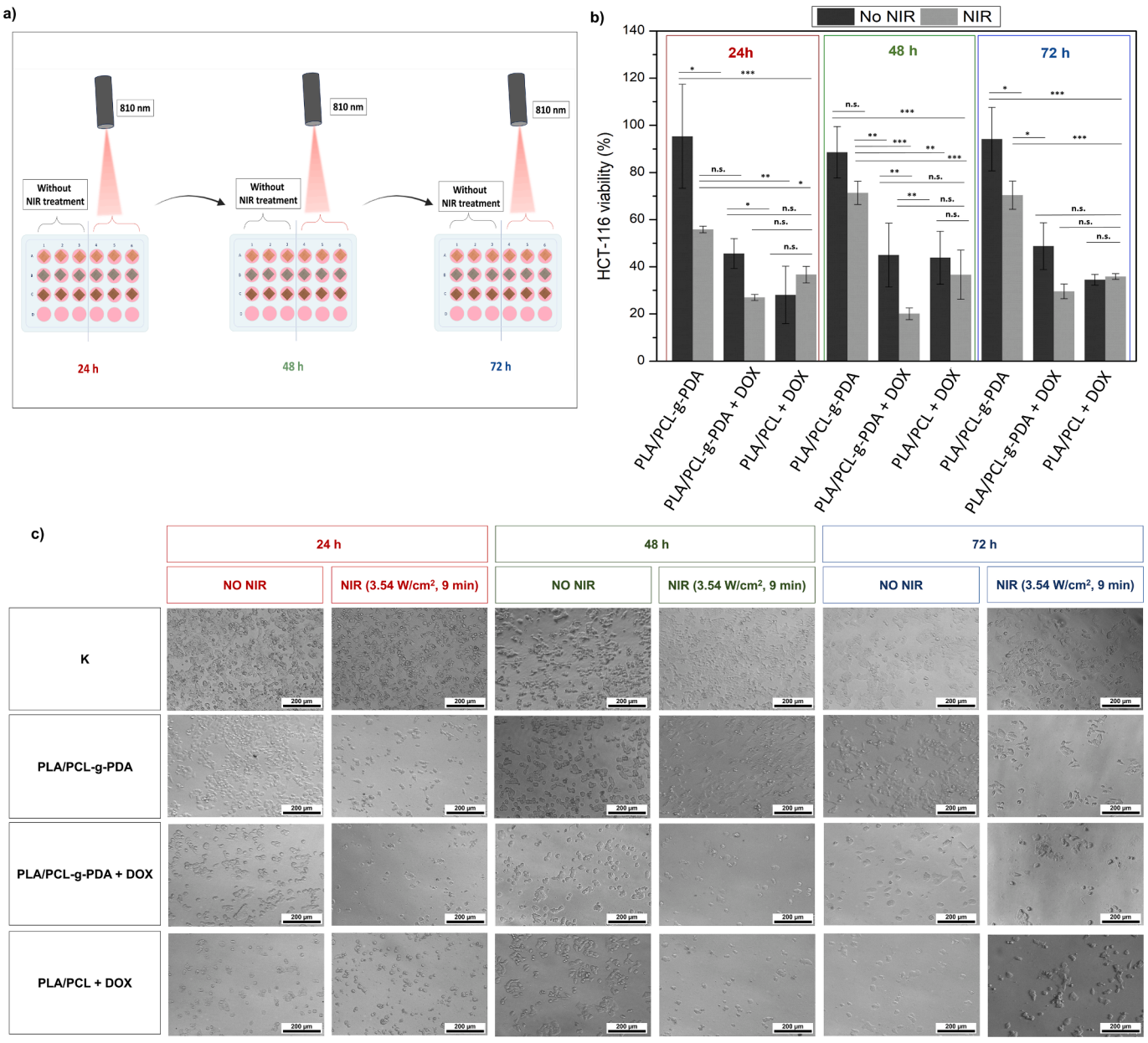

Fig. 6. Evaluation of the viability and morphology of HCT-116 cells cultured in the presence of electrospun scaffolds of different compositions. Experiment scheme (**a**) and cell viability (**b**) up to 72 h with PLA/PCL-g-PDA + DOX, PLA/PCL + DOX, and PLA/PCL-g-PDA scaffolds, comparing conditions with and without NIR laser irradiation (810 nm, 3.54 W/cm^2, 9 min/day). Optical microscopy images (**c**) show cell morphology after treatment with different scaffolds, both irradiated and non-irradiated. All data are shown as mean value ± SD (n = 3), (ns $p > 0.05$, *$p < 0.05$, **$p < 0.01$, ***$p < 0.001$).

scaffolds, as well as those exposed to irradiated PDA-containing samples, show clear morphological alterations and signs of cellular distress compared to negative controls of untreated cells.

Since the PLA/PCL-g-PDA + DOX scaffold had already demonstrated an enhanced cytotoxic effect due to DOX release and hyperthermia induced by NIR irradiation, its efficacy was further evaluated on 3D cultures of HCT-116 cells. It was chosen to test only the complete PLA/PCL-g-PDA + DOX scaffold with these 3D cultures as a proof-of-concept to validate the results obtained in the tests performed on 2D HCT-116 cultures. The resulting tumor spheroids were maintained for four days in the presence of the scaffold, under irradiated and non-irradiated conditions, using untreated spheroids as controls. Photothermal treatment was performed daily with NIR light (810 nm, 3.54 W/cm^2 for 9 min), and the volume of the spheroids was monitored as an indicator of the combined chemotherapeutic and photothermal activity. Furthermore, fluorescence microscopy images show that spheroids treated with PLA/PCL-g-PDA + DOX exhibited marked red fluorescence, indicative of intracellular incorporation of the released DOX (Fig. 7a). In untreated controls, volume progressively increased, while a moderate reduction was observed in spheroids exposed to the scaffold without irradiation, with an average volume of ~ 0.2 mm^3 after four days. Following NIR irradiation, volume further decreased to approximately ~ 0.05 mm^3, demonstrating an ablative effect (Fig. 7b). The reduction in spheroid volume, which after 4 days decreased to ~ 30% without NIR irradiation compared to control, was further accentuated, up to ~ 14% after NIR treatment. Overall, the marked reduction in spheroid volume after irradiation confirms the enhanced cytotoxic effect of chemotherapy and photothermal hyperthermia, demonstrating the potential of the scaffold as a combined system for anticancer treatment.

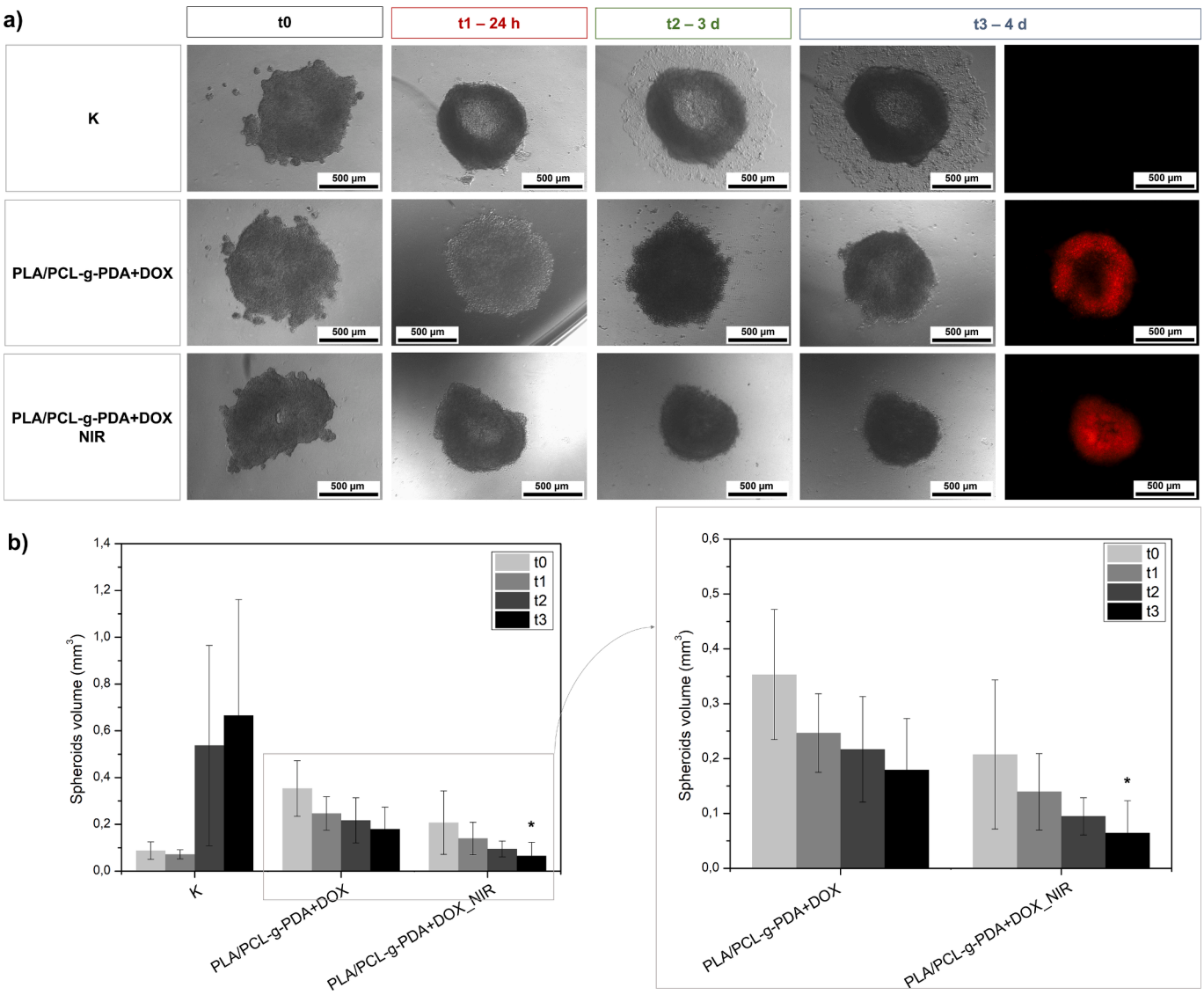

Fig. 7. Optical and fluorescence microscope images of spheroids (**a**) and reduction of their volume (**b**) after 4 days of incubation with PLA/PCL-g-PDA + DOX, also followed by NIR photothermal treatment (9 min, 3.54 W/cm^2, 810 nm). All data are shown as mean value ± SD (n = 3), (*p < 0.05).

4. Conclusions

The electrospinning technique allowed the production of a fibrillar scaffold based on PLA and the PCL-g-PDA copolymer, loaded with DOX. The use of hydrophobic polymers required low-pressure cold plasma treatment to improve surface wettability. Morphological analyses confirmed the correct formation of the electrospun fibers and the homogeneous distribution of the drug within the matrix. The use of PCL-g-PDA copolymer allowed the development of a photothermally active scaffold, capable of controlling release of DOX and inducing local hyperthermia under NIR irradiation, resulting in effective tumor cell ablation. Unlike traditional approaches based on PDA coatings or nanoparticles, the covalent bond ensures uniform distribution, high stability, and reproducible photothermal response. The results demonstrate that photothermal activity can be intrinsic to the material, opening up new perspectives in the design of multifunctional electrospun systems for advanced biomedical applications. The PLA/PCL-g-PDA + DOX scaffold therefore represents a multifunctional therapeutic system capable of integrating chemotherapy and photothermal therapy in a single platform. This combined therapeutic approach enhances cytotoxic efficacy while reducing potential systemic side effects, thanks to localized drug release at the tumor site. Overall, the results obtained highlight that one of the possible applications of the scaffold could be the potential locoregional treatment of cancer, with the prospect of improving post-surgical outcomes and reducing the risk of recurrence.

CRediT authorship contribution statement

Giuseppina Biscari: Writing – original draft, Validation, Software, Methodology, Investigation, Data curation, Conceptualization. **Alessia Lo Re:** Methodology, Investigation, Data curation. **Calogero Fiorica:** Writing – review & editing, Writing – original draft, Validation, Data curation, Conceptualization. **Vincent Darcos:** Conceptualization. **Stéphane Dejean:** Investigation. **Fabio Salvatore Palumbo:** Writing – review & editing, Conceptualization. **Gennara Cavallaro:** Writing – review & editing, Conceptualization. **Benjamin Nottelet:** Writing – review & editing, Conceptualization. **Giovanna Pitarresi:** Writing – review & editing, Funding acquisition, Conceptualization.

Declaration of competing interest

The authors declare that they have no known competing financial

interests or personal relationships that could have appeared to influence the work reported in this paper.

Appendix A. Supplementary data

Supplementary data to this article can be found online at https://doi.org/10.1016/j.ijpharm.2026.126689.

Data availability

Data will be made available on request.

References

Abasalta, M., Asefnejad, A., Khorasani, M.T., Saadatabadi, A.R., Irani, M., 2022. Adsorption and sustained release of doxorubicin from N-carboxymethyl chitosan/polyvinyl alcohol/poly(ε-caprolactone) composite and core-shell nanofibers. J. Drug Deliv. Sci. Technol. 67, 102937. https://doi.org/10.1016/J.JDDST.2021.102937.

Abbasi, N., Soudi, S., Hayati-Roodbari, N., Dodel, M., Soleimani, M., 2014. The effects of plasma treated electrospun nanofibrous poly (ε-caprolactone) scaffolds with different orientations on mouse embryonic stem cell proliferation. Cell J. (yakhteh) 16, 245.

Abounahia, N., Qiblawey, H., Zaidi, S.J., 2022. Progress for co-incorporation of polydopamine and nanoparticles for improving membranes performance. Membranes (basel) 12, 675. https://doi.org/10.3390/MEMBRANES12070675.

Aldhafeeri, T., Alotaibi, M., Barry, C.F., 2022. Impact of Melt Processing Conditions on the Degradation of Polylactic Acid. Polymers 2022, Vol. 14, Page 2790 14, 2790. Doi: 10.3390/POLYM14142790.

Atabey, M.E., Oncer, N., Yilmaz, A., Akinay, Y., Egri, S., Egri, O., Yilmaz, M., 2026. Silver nanostructure-decorated electrospun polycaprolactone Fibers as a potential wound dressing material. Chem. Phys. 601, 112969. https://doi.org/10.1016/J.CHEMPHYS.2025.112969.

Bahuon, F., Darcos, V., Patel, S., Marin, Z., Coudane, J., Schwach, G., Nottelet, B., 2022. Polyester-polydopamine copolymers for intravitreal drug delivery: role of polydopamine drug-binding properties in extending drug release. Biomacromolecules 23, 4388–4400. https://doi.org/10.1021/ACS.BIOMAC.2C00843/ASSET/IMAGES/LARGE/BM2C00843_0008.JPEG.

Biscari, G., Pitarresi, G., Fiorica, C., Schillaci, D., Catania, V., Palumbo, F.S., Giammona, G., 2022. Near-infrared light-responsive and antibacterial injectable hydrogels with antioxidant activity based on a Dopamine-functionalized Gellan Gum for wound healing. Int. J. Pharm. 627, 122257. https://doi.org/10.1016/J.IJPHARM.2022.122257.

Biscari, G., Sanz Del Olmo, N., Palumbo, F.S., Gaglio, R., Garofalo, G., Pitarresi, G., Fiorica, C., Malkoch, M., 2025. Antimicrobial NIR-Responsive Hydrogels based on Gellan Gum and Bis-MPA Polyester Dendrimers. ACS Appl. Mater. Interfaces 17, 22448–22463. https://doi.org/10.1021/ACSAMI.5C02386/ASSET/IMAGES/LARGE/AM5C02386_0011.JPEG.

Bu, L.L., Yan, J., Wang, Z., Ruan, H., Chen, Q., Gunadhi, V., Bell, R.B., Gu, Z., 2019. Advances in drug delivery for post-surgical cancer treatment. Biomaterials 219, 119182. https://doi.org/10.1016/J.BIOMATERIALS.2019.04.027.

Chen, W., Miao, H., Meng, G., Huang, K., Kong, L., Lin, Z., Wang, X., Li, X., Li, J., Liu, X.-Y., Lin, N., Chen, W., Miao, H., Meng, G.Q., Huang, K.L., Kong, L.Q., Lin, Z.F., Wang, X.D., Li, X.B., Li, J.H., Lin, N.B., Liu, X.-Y., 2022. Polydopamine-induced multilevel engineering of regenerated silk fibroin fiber for photothermal conversion. Small 18, 2107196. https://doi.org/10.1002/SMLL.202107196.

Chen, Y., Hou, Z., Liu, B., Huang, S., Li, C., Lin, J., 2015. DOX-Cu9S5@mSiO2-PG composite fibers for orthotopic synergistic chemo- and photothermal tumor therapy. Dalton Trans. 44, 3118–3127. https://doi.org/10.1039/C4DT03113J.

Dar, M.S., Rosaiah, P., Bhagyalakshmi, J., Ahirwar, S., Khan, A., Tamizhselvi, R., Reddy, V.R.M., Palaniappan, A., Sahu, N.K., 2025. Graphene quantum dots as nanotherapeutic agents for triple-negative breast cancer: Insights from 3D tumor models. Coord. Chem. Rev. 523, 216247. https://doi.org/10.1016/J.CCR.2024.216247.

Deng, Y., Yang, W.Z., Shi, D., Wu, M., Xiong, X.L., Chen, Z.G., Wei, S.C., 2019. Bioinspired and osteopromotive polydopamine nanoparticle-incorporated fibrous membranes for robust bone regeneration. NPG Asia Mater. 11, 1–13. https://doi.org/10.1038/S41427-019-0139-5;TECHMETA.

Ding, Y., Weng, L.-T., Yang, M., Yang, Z., Lu, X., Huang, N., Leng, Y., 2014. Insights into the Aggregation/deposition and Structure of a Polydopamine Film. https://doi.org/10.1021/LA5026608.

Doustgani, A., 2017. Doxorubicin release from optimized electrospun polylactic acid nanofibers. J. Ind. Text. 47, 71–88. https://doi.org/10.1177/1528083716634033.

Du, T., Yang, T., Xu, L., Li, X., Yang, G., Zhou, S., 2022. An implantable polydopamine nanoparticle-in-nanofiber device for synergistic cancer photothermal/chemotherapy. Adv. NanoBiomed Res. 2, 2200076. https://doi.org/10.1002/ANBR.202200076.

Esmaeili Ranjbar, A., Asadi, F., Mohandesnezhad, S., Vatanparast, M., Mohandesnezhad, S., Mirzaei, M.R., Noroozi Karimabad, M., Fathabadi, A.S., Esmaeili Ranjbar, F., 2025. Surface modification of electrospun polycaprolactone and zein using cold atmospheric plasma for tissue engineering applications. Sci. Rep. 15, 1–10. https://doi.org/10.1038/S41598-025-99450-6;SUBJMETA=166,301,357,54,639,985;KWRD=BIOMATERIALS, BIOMEDICAL+ENGINEERING, NANOSCALE+MATERIALS.

Federico, S., Martorana, A., Pitarresi, G., Palumbo, F.S., Fiorica, C., Giammona, G., 2022. Development of stimulus-sensitive electrospun membranes based on novel biodegradable segmented polyurethane as triggered delivery system for doxorubicin. Biomaterials Advances 136, 212769. https://doi.org/10.1016/J.BIOADV.2022.212769.

Feng, Y., Zhang, Z., Tang, W., Dai, Y., 2023. Gel/hydrogel-based in situ biomaterial platforms for cancer postoperative treatment and recovery. Exploration 3, 20220173. https://doi.org/10.1002/EXP.20220173.

Fernandes, N., Borges, S., Rodrigues, C.F., Correia, I.J., Moreira, A.F., 2025. Polydopamine-coated mesoporous silica/gold nanoclusters for enhanced chemo-photothermal therapy of cancer. Biomaterials Advances 177, 214405. https://doi.org/10.1016/J.BIOADV.2025.214405.

Fernández, J., Auzmendi, O., Amestoy, H., Diez-Torre, A., Sarasua, J.R., 2017. Mechanical properties and fatigue analysis on poly(ε-caprolactone)-polydopamine-coated nanofibers and poly(ε-caprolactone)-carbon nanotube composite scaffolds. Eur. Polym. J. 94, 208–221. https://doi.org/10.1016/J.EURPOLYMJ.2017.07.013.

Fiorica, C., Palumbo, F.S., Pitarresi, G., Biscari, G., Martorana, A., Calà, C., Maida, C.M., Giammona, G., 2021. Ciprofloxacin releasing gellan gum/polydopamine based hydrogels with near infrared activated photothermal properties. Int. J. Pharm. 610. https://doi.org/10.1016/j.ijpharm.2021.121231.

García-Mayorga, J.C., Rosu, H.C., Jasso-Salcedo, A.B., Escobar-Barrios, V.A., 2023. Kinetic study of polydopamine sphere synthesis using TRIS: relationship between synthesis conditions and final properties. RSC Adv. 13, 5081. https://doi.org/10.1039/D2RA06669F.

Han, X.J., Huang, Z.M., Huang, C., Du, Z.F., Wang, H., Wang, J., He, C.L., Wu, Q.S., 2012. Preparation and characterization of electrospun polyurethane/inorganic-particles nanofibers. Polym. Compos. 33, 2045–2057. https://doi.org/10.1002/PC.22348.

Hou, X., Guan, Y., Lu, Y., Wang, Y., Xu, S., Zhu, H., Zhao, J., Xiao, L., He, S., Shi, Y., 2025. Chitosan-based thermosensitive injectable hydrogel with hemostatic and antibacterial activity for preventing breast cancer postoperative recurrence and metastasis via chemo-photothermal therapy. Int. J. Biol. Macromol. 290, 138930. https://doi.org/10.1016/J.IJBIOMAC.2024.138930.

Hu, L., Ma, J., Wei, X., Li, Y., Jiang, S., Ji, X., Zhu, F., Tan, H., Wang, P., 2022. Biodegradable polydopamine and tetrasulfide bond co-doped hollowed mesoporous silica nanospheres as GSH-triggered nanosystem for synergistic chemo-photothermal therapy of breast cancer. Mater. Des. 215, 110467. https://doi.org/10.1016/J.MATDES.2022.110467.

Innocent Matumba, K., Clement Mokhena, T., Ojijo, V., Rotimi Sadiku, E., Sinha Ray, S., Matumba, K.I., Ojijo, V., Ray, S.S., Sadiku, E.R., Mokhena, T.C., 2024. Morphological characteristics, properties, and applications of polylactide/poly(ε-caprolactone) blends and their composites—a review. Macromol. Mater. Eng. 309, 2400056. https://doi.org/10.1002/MAME.202400056.

Ji, G., Zhang, Y., Si, X., Yao, H., Ma, S., Xu, Y., Zhao, J., Ma, C., He, C., Tang, Z., Fang, X., Song, W., Chen, X., 2021. Biopolymer immune implants' sequential activation of innate and adaptive immunity for colorectal cancer postoperative immunotherapy. Adv. Mater. 33, 2004559. https://doi.org/10.1002/ADMA.202004559;WEBSITE:WEBSITE:ADVANCED;CTYPE:STRING:JOURNAL.

Kaplan, J.A., Liu, R., Freedman, J.D., Padera, R., Schwartz, J., Colson, Y.L., Grinstaff, M. W., 2016. Prevention of lung cancer recurrence using cisplatin-loaded superhydrophobic nanofiber meshes. Biomaterials 76, 273–281. https://doi.org/10.1016/J.BIOMATERIALS.2015.10.060.

Khodadadi, M., Alijani, S., Montazeri, M., Esmaeilizadeh, N., Sadeghi-Soureh, S., Pilehvar-Soltanahmadi, Y., 2020. Recent advances in electrospun nanofiber-mediated drug delivery strategies for localized cancer chemotherapy. J. Biomed. Mater. Res. A 108, 1444–1458. https://doi.org/10.1002/JBM.A.36912.

Kim, S., Jeong, D.I., Karmakar, M., Huh, J.W., Hong, E.H., Kim, D.J., Ko, H.J., Cho, H.J., Lee, K.B., 2025. Multifunctional bioactive dual-layered nanofibrous matrix for effective breast cancer therapy and enhanced wound healing. Small 2500717. https://doi.org/10.1002/SMLL.202500717;WGROUP:STRING:PUBLICATION.

Langer, R., 1980. Invited review polymeric delivery systems for controlled drug release. Chem. Eng. Commun. 6, 1–48. https://doi.org/10.1080/00986448008912519.

Lee, H.A., Park, E., Lee, H., Lee, H.A., Park, E., Lee, H., 2020. Polydopamine and its derivative surface chemistry in material science: a focused review for studies at KAIST. Adv. Mater. 32, 1907505. https://doi.org/10.1002/ADMA.201907505.

Li, H., Zhu, J., Chen, S., Jia, L., Ma, Y., 2017a. Fabrication of aqueous-based dual drug loaded silk fibroin electrospun nanofibers embedded with curcumin-loaded RSF nanospheres for drugs controlled release. RSC Adv. 7, 56550–56558. https://doi.org/10.1039/C7RA12394A.

Li, W.Q., Wang, Z., Hao, S., He, H., Wan, Y., Zhu, C., Sun, L.P., Cheng, G., Zheng, S.Y., 2017b. Mitochondria-targeting polydopamine nanoparticles to deliver doxorubicin for overcoming drug resistance. ACS Appl. Mater. Interfaces 9, 16793–16802. https://doi.org/10.1021/ACSAMI.7B01540.

Link, S., Burda, C., Mohamed, M.B., Nikoobakht, B., El-Sayed, M.A., 1999. Laser photothermal melting and fragmentation of gold nanorods: energy and laser pulse-width dependence. J. Phys. Chem. A 103. https://doi.org/10.1021/JP983141K/ASSET/IMAGES/LARGE/JP983141KF00004.JPEG.

Liu, J., Wang, K., Jin, F., Bin, Y., Li, J., Qian, X., 2025. Advances in Photothermal Electrospinning: From Fiber Fabrication to Biomedical Application. Polymers 2025, Vol. 17, Page 1725 17, 1725. Doi: 10.3390/POLYM17131725.

Liu, Z., Zhang, Y., Yin, H., Geng, X., Li, S., Zhao, J., Zeng, Z., Ye, X., Yu, J., Feng, F., Kang, W., 2022. Comparison of prognosis between microscopically positive and negative surgical margins for primary gastrointestinal stromal tumors: a systematic review and meta-analysis. Front. Oncol. 12, 679115. https://doi.org/10.3389/FONC.2022.679115/BIBTEX.

MacKey, M.A., Ali, M.R.K., Austin, L.A., Near, R.D., El-Sayed, M.A., 2014. The most effective gold nanorod size for plasmonic photothermal therapy: Theory and in vitro experiments. J. Phys. Chem. B 118, 1319–1326. https://doi.org/10.1021/JP409298F/SUPPL_FILE/JP409298F_SI_001.PDF.

Mahmoud, N.N., Aqabani, H., Hikmat, S., Abu-Dahab, R., 2021. Colloidal stability and cytotoxicity of polydopamine-conjugated gold nanorods against prostate cancer cell lines. Molecules 26, 1299. https://doi.org/10.3390/MOLECULES26051299.

Martorana, A., Puleo, G., Miceli, G.C., Cancilla, F., Licciardi, M., Pitarresi, G., Tranchina, L., Marrale, M., Palumbo, F.S., 2025. Redox/NIR dual-responsive glutathione extended polyurethane urea electrospun membranes for synergistic chemo-photothermal therapy. Int. J. Pharm. 669, 125108. https://doi.org/10.1016/J.IJPHARM.2024.125108.

Min, K.-E.;, Jang, J.-W.;, Kim, C ;, Yi, S, Min, K.-E., Jang, J.-W., Kim, Cheolhee, Yi, Sung, 2024. Enhancement of Mechanical Properties of PCL/PLA/DMSO2 Composites for Bone Tissue Engineering. Applied Sciences 2024, Vol. 14, Page 6190 14, 6190. Doi: 10.3390/APP14146190.

Pitarresi, G., Barberi, G., Palumbo, F.S., Schillaci, D., Fiorica, C., Catania, V., Indelicato, S., Bongiorno, D., Biscari, G., Giammona, G., 2022. Developing Antibiofilm Fibrillar Scaffold with Intrinsic Capacity to produce Silver Nanoparticles. Int. J. Mol. Sci. 23, 15378. https://doi.org/10.3390/IJMS232315378/S1.

Rezk, A.I., Lee, J., Kim, B.S., Chun, S., 2024. Strategically designed bifunctional polydopamine enwrapping polycaprolactone-hydroxyapatite-doxorubicin composite nanofibers for osteosarcoma treatment and bone regeneration. ACS Appl. Mater. Interfaces 16. https://doi.org/10.1021/ACSAMI.4C03015.

Shafique, M., Ur Rehman, M., Kamal, Z., Alzhrani, R.M., Alshehri, S., Alamri, A.H., Bakkari, M.A., Sabei, F.Y., Safhi, A.Y., Mohammed, A.M., Hamd, M.A.E., Almawash, S., 2023. Formulation development of lipid polymer hybrid nanoparticles of doxorubicin and its in-vitro, in-vivo and computational evaluation. Front. Pharmacol. 14, 1025013. https://doi.org/10.3389/FPHAR.2023.1025013/FULL.

Sun, M., Downes, S., 2009. Physicochemical characterisation of novel ultra-thin biodegradable scaffolds for peripheral nerve repair. Journal of Materials Science: Materials in Medicine 2009 20:5 20, 1181–1192. doi: 10.1007/S10856-008-3671-3.

Sung, H., Ferlay, J., Siegel, R.L., Laversanne, M., Soerjomataram, I., Jemal, A., Bray, F., 2021. Global Cancer Statistics 2020: GLOBOCAN estimates of Incidence and Mortality Worldwide for 36 Cancers in 185 Countries. CA Cancer J. Clin. 71, 209–249. https://doi.org/10.3322/CAAC.21660.

Sy, K.H.S., Ho, L.W.C., Lau, W.C.Y., Ko, H., Choi, C.H.J., 2018. Morphological Diversity, Protein Adsorption, and Cellular Uptake of Polydopamine-Coated Gold Nanoparticles. Langmuir 34, 14033–14045. https://doi.org/10.1021/ACS.LANGMUIR.8B02572.

Tiwari, A.P., Bhattarai, D.P., Maharjan, B., Ko, S.W., Kim, H.Y., Park, C.H., Kim, C.S., 2019. Polydopamine-based implantable multifunctional nanocarpet for highly efficient photothermal-chemo therapy. Sci. Rep. 9, 1–13. https://doi.org/10.1038/S41598-019-39457-Y;TECHMETA=128,145;SUBJMETA=152,2733,352,639,925;KWRD=DRUG+DELIVERY, NANOTECHNOLOGY+IN+CANCER.

Tran, T.H., Nguyen, H.T., Pham, T.T., Choi, J.Y., Choi, H.G., Yong, C.S., Kim, J.O., 2015. Development of a Graphene Oxide Nanocarrier for Dual-Drug Chemo-phototherapy to Overcome Drug Resistance in Cancer. ACS Appl. Mater. Interfaces 7, 28647–28655. https://doi.org/10.1021/ACSAMI.5B10426.

Wang, X., Wu, B., Zhang, Y., Dou, X., Zhao, C., Feng, C., 2022. Polydopamine-doped supramolecular chiral hydrogels for postoperative tumor recurrence inhibition and simultaneously enhanced wound repair. Acta Biomater. 153, 204–215. https://doi.org/10.1016/J.ACTBIO.2022.09.012.

Xu, R., Xie, J., Lei, C., 2017. Influence of melt-draw ratio on the crystalline behaviour of a polylactic acid cast film with a chi structure. RSC Adv. 7, 39914–39921. https://doi.org/10.1039/C7RA05422J.

Yan, J., Huang, Y., Miao, Y.E., Tjiu, W.W., Liu, T., 2015. Polydopamine-coated electrospun poly(vinyl alcohol)/poly(acrylic acid) membranes as efficient dye adsorbent with good recyclability. J. Hazard. Mater. 283, 730–739. https://doi.org/10.1016/J.JHAZMAT.2014.10.040.

Yang, D.H., Lee, N.Y., 2024. Electrospun fibers modified with polydopamine for enhancing human mesenchymal stem cell culture. Biomed. Mater. 19, 045012. https://doi.org/10.1088/1748-605X/AD49F7.

Yao, Q., Cosme, J.G.L., Xu, T., Miszuk, J.M., Picciani, P.H.S., Fong, H., Sun, H., 2017. Three dimensional electrospun PCL/PLA blend nanofibrous scaffolds with significantly improved stem cells osteogenic differentiation and cranial bone formation. Biomaterials 115, 115–127. https://doi.org/10.1016/J.BIOMATERIALS.2016.11.018.

Zhang, J., Wang, X., Liu, T., Liu, S., Jing, X., 2016. Antitumor activity of electrospun polylactide nanofibers loaded with 5-fluorouracil and oxaliplatin against colorectal cancer. Drug Deliv. 23, 794–800. https://doi.org/10.3109/10717544.2014.916768.

Zhang, L., Wu, B., Zha, Z., Zhao, H., Jiang, Y., Yuan, J., 2018. Positive surgical margin is associated with biochemical recurrence risk following radical prostatectomy: a meta-analysis from high-quality retrospective cohort studies. World J. Surg. Oncol. 16, 1–12. https://doi.org/10.1186/S12957-018-1433-3/FIGURES/5.

Zhang, Y., Jiang, C., 2021. Postoperative cancer treatments: In-situ delivery system designed on demand. J. Control. Release 330, 554–564. https://doi.org/10.1016/J.JCONREL.2020.12.038.

Zhou, J.J., Feng, Y.C., Zhao, M.L., Guo, Q., Zhao, X.B., 2025. Nanotechnology-driven strategies in postoperative cancer treatment: innovations in drug delivery systems. Front. Pharmacol. 16, 1586948. https://doi.org/10.3389/FPHAR.2025.1586948/XML.